

High-precision measurement of the complex magneto-optical Kerr effect using weak measurement

Tong Li^{1, a)}, Yunhan Wang^{1, a)}, Yinghang Jiang¹, Sijie Zhang^{1, 2}, Lan Luo^{3, 4, 5} and Zhiyou Zhang¹

¹⁾College of Physics, Sichuan University, Chengdu, Sichuan 610065, China

²⁾Guizhou University of Engineering Science, Bijie, Guizhou 551700, China

³⁾the National Key Laboratory of Optical Field Manipulation Science and Technology, Chinese Academy of Sciences, Chengdu 610209, China

⁴⁾Key Laboratory of Science and Technology on Space Optoelectronic Precision Measurement, Chinese Academy of Sciences, Chengdu, Sichuan 610209, China

⁵⁾Institute of Optics and Electronics, Chinese Academy of Sciences, Chengdu, Sichuan 610209, China

(*Corresponding author: zhangzhiyou@scu.edu.cn)

(*Corresponding author: naloul@163.com)

The present paper introduces a quantum weak measurement (WM) scheme for the measurement of the complex magneto-optical Kerr effect (MOKE). We achieve the simultaneous measurement of the Kerr rotation angle and the ellipticity in a single WM process by utilizing two auxiliary pointers derived from the same meter state. The experimental measurement precision for both the Kerr rotation angle and the ellipticity is capable of reaching 10^{-4} deg. This technique is also employed for the determination of the complex magneto-optical constant Q . The proposed method overcomes the limitation of acquiring the complex magneto-optical Kerr parameters through a multi-step measurement process, which was previously encountered. This breakthrough holds immense significance for efficiently measuring and applying the complex MOKE with high precision and cost-effectiveness.

The magneto-optical Kerr effect (MOKE), which originates from the anisotropy of the dielectric tensor¹, refers to the phenomenon that when a linear polarized beam incident on the interface of a magnetic medium, the polarization state or the intensity of the reflected light is changed. The corresponding magneto-optical Jones matrix used to characterize this effect can be represent as

$$\mathfrak{R}_1 = \begin{bmatrix} r_{pp} & r_{ps} \\ r_{sp} & r_{ss} \end{bmatrix}, \quad (1)$$

where r_{pp} , r_{ps} , r_{sp} and r_{ss} are the Fresnel coefficients of the magnetic medium². There are three cases of MOKE depending on the orientation of the magnetization relative to the interface, the polar magneto-optical Kerr effect (PMOKE), the longitudinal magneto-optical Kerr effect (LMOKE), and the transverse magneto-optical Kerr effect (TMOKE)^{2,3}. Among them, both LMOKE and PMOKE cause changes in the polarization state of the reflected light. This process can be expressed by the complex magneto-optical Kerr angle

$$\Theta_K = \theta_K - i\varepsilon_K, \quad (2)$$

where the real and the imaginary part of it represent the Kerr optical rotation angle and the Kerr ellipticity of the reflected polarization, respectively. Without loss of generality, for horizontal polarization $|H\rangle$, it gives $\Theta_K^H = r_{sp}/r_{pp}$, while for vertical polarization $|V\rangle$, it becomes $\Theta_K^V = r_{ps}/r_{ss}$.

With the development of spintronics, MOKE especially the longitudinal and the polar configuration has shown the superiority for the in-situ investigation of the magnetic properties of magneto-optical devices and thin films, and has been

widely applied in magnetism measurement⁴, magnetic domain imaging^{5,6}, magneto-optical ellipsometry^{7,8}, magneto-optical recording⁹, etc., because θ_K and ε_K are highly sensitive to the magnetization \mathbf{M} of the magnetic materials.

In recent years, some studies used weak measurement (WM) to measure the tiny MOKE signals of separate θ_K and ε_K ¹⁰⁻¹⁴, which has the advantages of high precision and cost-effectiveness. WM is a technique for the measurement of high-precision parameters by amplifying the observables. It includes the processes of pre-selection, weak coupling, and post-selection. It was first proposed by Aharonov, Albert, and Vaidman in 1988¹⁵. Since WM improves the signal-to-noise ratio significantly and has extremely high sensitivity, it has been used in the detection of beam shift¹⁶⁻¹⁹, frequency²⁰, optical phases²¹⁻²³, chirality²⁴⁻²⁶, chemical reaction processes^{27,28}, angular rotations²⁹, refractive index^{30,31}, optical conductivity³², and phase transition process³³, etc.

To study the complex MOKE and apply it to the investigations of materials' properties, e.g., the measurement of the complex optical parameters, both θ_K and ε_K are required to be measured quantitatively. However, θ_K and ε_K always coexist and simultaneously contribute to the detected MOKE signals. In the previous work, these two parameters have to be measured separately by using and adjusting the angle of a quarter-wave-plate both in the traditional MOKE setup³⁴ and the WM method¹⁰. It not only decreases the measurement efficiency, but also brings an extra error given by the separate measurement processes. Although the measurement efficiency can be improved by splitting the reflected light into multiple beams and obtaining the signals of θ_K and ε_K simultaneously through different post-selection processes^{35,36}, these two parameters are still measured by two meter states, which introduces added intricacy and raises the expenses of the optical system.

^{a)}These authors contributed equally to this work.

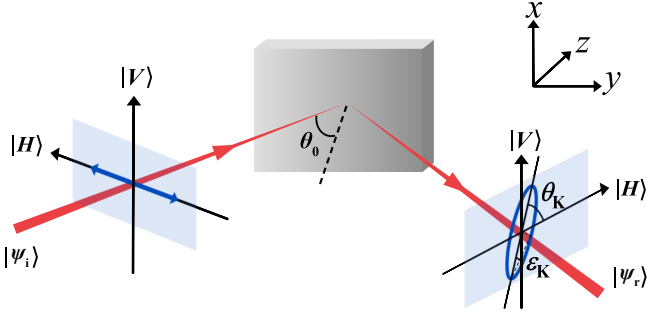


FIG. 1. Diagram of a polarized beam incident on the interface of a magnetic film with the incident angle of θ_0 . Due to MOKE, the polarization of the light undergoes a transformation from the state $|\psi_i\rangle$ to $|\psi_r\rangle$. θ_K and ϵ_K denote the Kerr optical rotation angle and the Kerr ellipticity of the reflected polarization, respectively.

In this work, we propose a scheme to measure the complex MOKE using WM. For the pre-selection, the polarized light beam is reflected normally from the magnetic film, in which configuration the induced MOKE is widely applied in high-density storage and measurement of the pure PMOKE^{37,38}. Next, a glass prism is used to induce the spin Hall effect of light (SHEL), which serves as the weak coupling. After the post-selection, we introduce two auxiliary pointers given by the final meter state to characterize the complex MOKE signal. The simultaneous measurement of θ_K and ϵ_K in a single WM process is theoretically and experimentally realized. Compared to the previous methods of separately measuring these two parameters, this scheme greatly improves the efficiency and precision. Further, the complex magneto-optical constant Q , a coefficient to characterize the intrinsic magneto-optical property of the material, is also calculated in our experiment as an application of this technique. Other applications that are significant to the exploration of the complex MOKE, such as the manipulation of SHEL through an applied magnetic field³⁹, are attainable as well in our scheme.

Considering an initialized horizontal polarization $|\psi_i\rangle = |H\rangle$ reaching a magnetic interface from a nonmagnetic medium, as shown in Fig. 1, MOKE occurs and the state of the reflected light (the space part is omitted here) gives

$$\begin{aligned} |\psi_r^1\rangle &= r_{pp}|H\rangle + r_{sp}|V\rangle \\ &\approx \frac{r_{pp}}{\sqrt{2}} \left[e^{-i\theta_K - \epsilon_K}|+\rangle + e^{i\theta_K + \epsilon_K}|-\rangle \right], \end{aligned} \quad (3)$$

where $|+\rangle = (|H\rangle + i|V\rangle)/\sqrt{2}$ and $|-\rangle = (|H\rangle - i|V\rangle)/\sqrt{2}$ are the left- and the right-circular polarization states, respectively. In the second line of Eq. (3), the approximation condition $|r_{sp}/r_{pp}| = |\theta_K - i\epsilon_K| \ll 1$ is used in the calculation. For normal incidence we interested in, the complex MOKE angle can be expressed by²

$$\Theta_K^H = \theta_K - i\epsilon_K = \frac{r_{sp}}{r_{pp}} = \frac{in_0n_1Qm_z}{n_1^2 - n_0^2}, \quad (4)$$

where n_0 , n_1 are the refractive indices of the nonmagnetic medium, and that of the magnetic medium, respectively. m_z is

a direction cosine of the magnetization \mathbf{M} . $Q = Q_0 \exp(-iq)$ is the complex magneto-optical constant, whose amplitude Q_0 is proportional to the magnetization intensity³ and q is its phase factor. In addition, it should be emphasized that r_{pp} is a constant in this configuration.

Previous weak measurement scheme for measuring MOKE usually employ the SHEL induced by the magnetic sample as the weak coupling^{1,13,14}. However, SHEL only exists with oblique incidence⁴⁰, therefore, we consider the case that the light undergoes a second reflection from a prism obliquely with the incident angle of θ_i to excite SHEL in the air-glass interface as the weak coupling, which takes the form

$$\hat{U}_{\text{int}} = \exp(-i\delta\hat{\sigma}_3k_y), \quad (5)$$

where $\hat{\sigma}_3 = |+\rangle\langle+| - |-\rangle\langle-|$, the spin operator of a photon, is the observable of the quantum system being measured, k_y is the transverse component of the wave vector describing the momentum wave function, and $\delta = (1 + r_s/r_p) \cot \theta_i/k$ represents the photon spin splitting occurring on the air-glass interface¹⁶, which is used to reflect the strength of the spin-orbit coupling between $\hat{\sigma}_3$ and k_y . After that interaction, the polarization and the space parts of the light are entangled, and the total state of the second reflected light gives

$$\begin{aligned} |\psi_r^2\rangle &= \exp(-i\delta\hat{\sigma}_3k_y)\mathfrak{R}_2|\psi_r^1\rangle|\phi\rangle \\ &= \exp(-i\delta\hat{\sigma}_3k_y)|\psi_{\text{pre}}\rangle|\phi\rangle, \end{aligned} \quad (6)$$

where $|\phi\rangle = \int dk_y (w/\sqrt{2\pi})^{1/2} \exp(-w^2k_y^2/4) |k_y\rangle$ is the momentum wave function with Gaussian distribution (w denotes the beam waist), which serves as the meter in the WM scheme. Unlike Eq. (1) which has non-diagonal elements,

$$\mathfrak{R}_2 = \begin{bmatrix} r_p & 0 \\ 0 & r_s \end{bmatrix}, \quad (7)$$

is the Jones matrix describing the reflection upon an isotropic non-magnetic dielectric medium (glass), and $|\psi_{\text{pre}}\rangle = \mathfrak{R}_2|\psi_r^1\rangle$ is regarded as the pre-selected state in the WM system.

Next, the state of the whole system undergoes a free evolution $\hat{U}_{\text{free}} = \exp(-ik_y^2z/2k)$ (z is the free propagation distance)¹⁶, and during this process, it is post-selected on the state

$$|\psi_{\text{post}}\rangle = |V\rangle = -\frac{i}{\sqrt{2}}(|+\rangle - |-\rangle). \quad (8)$$

Therefore, the final wave function of the light in the momentum space gives

$$\begin{aligned} |\Phi\rangle &= \hat{U}_{\text{free}}|\psi_{\text{post}}\rangle\langle\psi_{\text{post}}|\exp(-i\delta\hat{\sigma}_3k_y)|\psi_{\text{pre}}\rangle|\phi\rangle \\ &= \hat{U}_{\text{free}}\langle\psi_{\text{post}}|\psi_{\text{pre}}\rangle[\cos(\delta k_y) - iA_w \sin(\delta k_y)]|\phi\rangle|\psi_{\text{post}}\rangle, \end{aligned} \quad (9)$$

where

$$A_w = \frac{\langle\psi_{\text{post}}|\hat{\sigma}_3|\psi_{\text{pre}}\rangle}{\langle\psi_{\text{post}}|\psi_{\text{pre}}\rangle} = \frac{r_p \sinh 2\epsilon_K - i \sin 2\theta_K}{r_s \cos 2\theta_K - \cosh 2\epsilon_K} \quad (10)$$

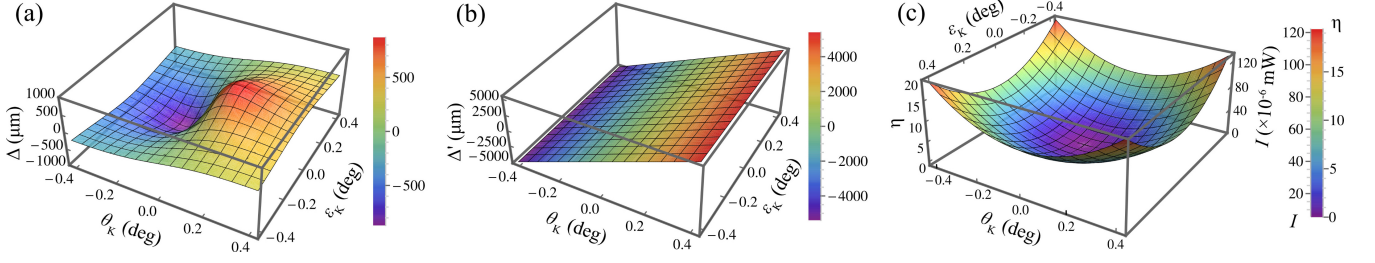


FIG. 2. Theoretical dependencies of the pointers on the complex MOKE. (a) and (b) are the amplified shift Δ , and the modified shift Δ' with the two MOKE parameters (i.e., θ_K and ϵ_K). Δ' shows a higher dynamic measurement range with wider consistent sensitivity compared with Δ (the standard WM scheme). (c) shows the curve of the relative intensity change η along with the post-selected intensity I , where the left and right scales of the color bar represents the values of I and η , respectively. The parameters taken in the plots correspond to the experiment settings.

is the complex weak value corresponding to the complex MOKE. What noteworthy is that when only Kerr optical rotation angle θ_K (Kerr ellipticity ϵ_K) appears, the complex A_w

degenerates into a pure imaginary (real) one.

And the amplified shift of the beam, which is the most currently used pointer in WM, can be calculated as

$$\begin{aligned} \Delta|_{\theta_K, \epsilon_K} &= \frac{\langle \Phi | \hat{y} | \Phi \rangle}{\langle \Phi | \Phi \rangle} = \frac{\int_{-\infty}^{+\infty} \Phi^*(k_y) i \partial k_y \Phi(k_y) dk_y}{\int_{-\infty}^{+\infty} \Phi^*(k_y) \Phi(k_y) dk_y} \\ &\approx \frac{z}{R_0} \frac{2r_s r_p \delta \sin 2\theta_K}{[r_s^2 - r_p^2 + e^{k_0 \delta^2 / R_0} (r_s^2 + r_p^2)] \cosh 2\epsilon_K - [r_s^2 + r_p^2 + e^{k_0 \delta^2 / R_0} (r_s^2 - r_p^2)] \cos 2\theta_K}, \end{aligned} \quad (11)$$

where $R_0 = kw^2/2$ is the Rayleigh distance. The theoretical relationship between Δ and the complex MOKE is shown in Fig. 2(a). It can be seen that the role of ϵ_K is almost ignored when the complex MOKE signal is weak enough. Thus, the pointer Δ is used to measure weak θ_K in previous literature¹⁰. However, the linearity of Δ with θ_K decreases with the increasing of θ_K , and is affected by the value of ϵ_K . For the

general cases, the max value of θ_K that keeps a good linearity with Δ are on the order of 10^{-2} deg (see the supplementary material for details). This limitation restricts practical applications. Moreover, it is hard to provide the information about ϵ_K when employing Δ as the only pointer.

To obtain more information of the complex MOKE, we introduce the post-selected intensity as an extra pointer:

$$\begin{aligned} I|_{\theta_K, \epsilon_K} &\propto \langle \Phi | \Phi \rangle = \int_{-\infty}^{+\infty} \Phi^*(k_y) \Phi(k_y) dk_y \\ &\propto [r_s^2 - r_p^2 + e^{k_0 \delta^2 / R_0} (r_s^2 + r_p^2)] \cosh 2\epsilon_K - [r_s^2 + r_p^2 + e^{k_0 \delta^2 / R_0} (r_s^2 - r_p^2)] \cos 2\theta_K. \end{aligned} \quad (12)$$

It contains the information of both θ_K and ϵ_K but dependent non-linearly with neither of them.

By combining Eq. (11) and (12), we can derive two auxiliary pointers, the modified shift Δ' and the relative intensity change η , to characterize the complex MOKE. They take the following forms:

$$\Delta'|_{\theta_K} = \frac{I|_{\theta_K, \epsilon_K}}{I|_{\theta_K=0, \epsilon_K=0}} \cdot \Delta \approx \frac{2zr_s}{k\delta r_p} \theta_K, \quad (13)$$

$$\eta|_{\theta_K, \epsilon_K} = \frac{I|_{\theta_K, \epsilon_K} - I|_{\theta_K=0, \epsilon_K=0}}{I|_{\theta_K=0, \epsilon_K=0}} \approx \frac{r_s^2 w^2}{r_p^2 \delta^2} (\theta_K^2 + \epsilon_K^2), \quad (14)$$

where $I|_{\theta_K=0, \epsilon_K=0}$ is the post-selected intensity corresponding to no polarization change. The approximations in Eq. (13) and (14) are valid when $|\theta_K - i\epsilon_K| \ll 1$ (subtle MOKE signal), and $|\delta/w| \ll 1$ (weak coupling condition). The theoretical dependencies of the two auxiliary pointers and the complex MOKE are shown in Fig. 2(b) and Fig. 2(c). It can be seen that the

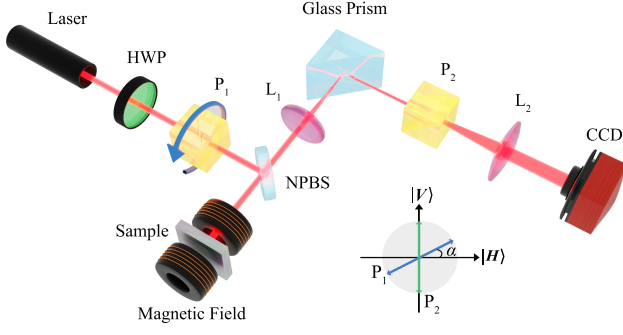


FIG. 3. Experiment setup for the measurement of the complex MOKE. The light source is a He-Ne laser (wavelength = 623.8 nm), HWP is a half-wave plate, P_1 and P_2 are Glan laser polarizers, NPBS is a non-polarizing beam splitter, L_1 and L_2 are the lenses with the focal lengths of 50 mm and 250 mm respectively, CCD denotes the charge-coupled device. The inset shows the polarization states prepared by P_1 and P_2 . The optical axis of P_1 deviates an angle of α from $|H\rangle$, while the optical axis of P_2 is parallel to $|V\rangle$.

value of Δ' is merely dependent on θ_K and the linearity maintains in the whole area. Compared to the Δ pointer for measuring θ_K , the Δ' pointer greatly enlarge the linear response region. η is linear to I and determined by both of θ_K and ϵ_K , which is used for the calculation of ϵ_K . Thus, θ_K and ϵ_K can be obtained using these two auxiliary pointers in a single WM process. It is worthy noting that the values of all the pointers are at the minimum when MOKE is absent.

The experimental measurement system is shown in Fig. 3. The light source is a He-Ne laser (Thorlabs HNL210) with a wavelength of 632.8 nm, which passes through a half-wave plate (HWP) to adjust the intensity. Next, the light beam passes through a Glan polarizer (P_1 , extinction ratio 100 000 : 1). Since standard WM scheme provides the best sensitivity for the measurement of θ_K when the pre-selected state is parallel to $|H\rangle$, where Δ is 0. Thus, we adjust P_1 and obtain the initial polarization state $|\psi_i\rangle = |H + \alpha\rangle$, where $\alpha = \theta_{K0}$ is an auxiliary compensation angle used to offset the initial Kerr rotation angle θ_{K0} (see the supplementary material for details). Then, the beam passes through the non-polarizing beam splitter (NPBS) and normally reaches to the surface of the magnetic thin film, to which the external magnetic field B is applied perpendicular. Then, the reflected light is focused by a lens L_1 ($f = 50$ mm) and then reflected obliquely from the BK-7 glass prism. The incident angle $\theta_i = 40^\circ$ is kept throughout the experiment. With this photon wavelength and incident angle, the refractive index of the glass prism is 1.51. r_p and r_s are 0.122 and -0.282 , respectively. A lens L_2 ($f = 250$ mm) is used to generate the free propagation amplification¹⁶ on the beam and another Glan polarizer (P_2 , extinction ratio 100 000 : 1) is used to prepare $|\psi_{\text{post}}\rangle = |V\rangle$ as the post-selected state. The detection of the reflected beam is finally carried out using a charge coupled device (CCD, WORK POWER WP-UT400).

A Ni-Fe film with the thickness of 30 nm that depositing on the silicon substrate using the vacuum thermal evaporation

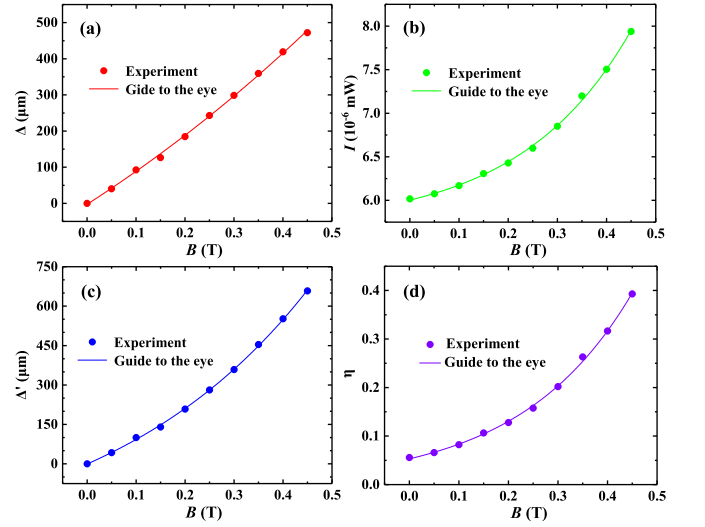


FIG. 4. The dependence of the pointers and the intensity of the magnetic field. (a) and (b) are the experiment results for the measurement of Δ and I , under room temperature. (c) and (d) show the two auxiliary pointers Δ' and η calculated by the measurement results. The scatters are the average values of the measurement, and the curves are the guides to the eye.

technique is prepared for the experiment. During the measurement, the applied magnetic field B is changed from 0 to 0.45 T with steps of 0.05 T. At each value of B , the amplified shift Δ and the post-selected intensity I are recorded 30 times with intervals of 1 second by the CCD. The measurement results of Δ and I are shown in Fig. 4(a) and 4(b). It can be seen that both Δ and I increase with the increase of B , due to the increase of θ_K and ϵ_K , which is consistent with our theory. Fig. 4(c) and 4(d) show the two auxiliary pointers calculated by the experiment results. Here, the post-selected intensity without MOKE $I|_{\theta_K=0, \epsilon_K=0} = 5.7 \times 10^{-6}$ mW is determined by measuring the minimum value of I while changing B , under the condition of $|\psi_i\rangle = |H\rangle$. Except for this used method, it can also be determined by employing a quarter-wave-plate to compensate the ellipticity, while adjusting the angle of P_1 to compensate the rotation angle.

Furthermore, we can characterize the complex MOKE using the two auxiliary pointers. According to Eq. (13) and Eq. (14), the expressions of θ_K (with the initial θ_{K0}) and ϵ_K are

$$\theta_K|_{\Delta', \alpha} = \frac{k\delta r_p}{2zr_s} \Delta' + \theta_{K0}|\alpha, \quad (15)$$

$$\epsilon_K|_{\Delta', \eta} = \sqrt{\frac{r_p^2 \delta^2}{r_s^2 w^2} \eta - \left(\frac{k\delta r_p}{2zr_s} \Delta'\right)^2}. \quad (16)$$

In this experiment, $\theta_{K0} = \alpha = 0.035$ deg. Thus, we can calculate the dependence of the complex MOKE on B , which are shown in Fig. 5(a). It can be seen that both of the two parameters increase with the increasing of B . The measurement

precision of these two parameters can be evaluated by

$$S_{\theta_K} = \sqrt{\left(\frac{\partial \theta_K}{\partial \Delta} S_{\Delta}\right)^2 + \left(\frac{\partial \theta_K}{\partial I} S_I\right)^2 + \left(\frac{\partial \theta_K}{\partial I_0} S_{I_0}\right)^2}, \quad (17)$$

$$S_{\varepsilon_K} = \sqrt{\left(\frac{\partial \varepsilon_K}{\partial \Delta} S_{\Delta}\right)^2 + \left(\frac{\partial \varepsilon_K}{\partial I} S_I\right)^2 + \left(\frac{\partial \varepsilon_K}{\partial I_0} S_{I_0}\right)^2}, \quad (18)$$

where S_{Δ} , S_I , S_{I_0} are the standard deviations of Δ , I , and I_0 , respectively. In this experiment, $S_{\Delta} \approx 2.5 \mu\text{m}$ and $S_{I_0} \approx S_I \approx 0.013 \times 10^{-6} \text{ mW}$ are calculated by the 30 times measurement. Thus, the corresponding standard derivations of θ_K and ε_K , $S_{\theta_K} \approx S_{\varepsilon_K} \approx 2.5 \times 10^{-4} \text{ deg}$, are obtained (see the supplementary material for details).

Furthermore, we calculate the complex magneto-optical constant Q using this method. From Eq. (4), Q can be calculated as

$$Q = \frac{(n_1^2 - n_0^2)(\varepsilon_K - i\theta_K)}{n_0 n_1 m_z}. \quad (19)$$

Since the plane of the Ni-Fe film is isotropic, and the applied magnetic field is normal to the film surface, we assume $m_z = 1$ during the whole measurement process. The refractive indices of n_0 and n_1 are 1 and $1.26 - 0.44i$, respectively, where n_1 is measured by the ellipsometer. We depict the dependence of Q and B , as shown in Fig. 5(b). The amplitude Q_0 intuitively shows the magnetization performance perpendicular to the film surface, while the phase q remains a constant.

In summary, we propose a method to measure the complex MOKE using WM. By introducing two auxiliary pointers, Δ' and η , we realize the simultaneous measurement of θ_K and ε_K with the precision of $2.5 \times 10^{-4} \text{ deg}$, which addressed the problem that these two MOKE parameters have to be measured separately using previous methods. Since the information of the two pointers are given by the same meter state, this scheme greatly improve the efficiency and precision for the measurement of the complex optical parameters. It is worthy noting that a higher measurement precision could be further achieved by combing with the quantum light source or the noise reduction techniques such as the lock-in amplifier. What's more, since the complex MOKE cause a rotation angle and an ellipticity of the polarization light before it reached to the surface where SHEL occurs, it can be used as a flexible approach to manipulate the spin splitting of SHEL with quantitative analysis.

SUPPLEMENTARY MATERIAL

See the supplementary material for (S1) feasibility of introducing the compensation angle α , (S2) calculation of the measurement precision of θ_K and ε_K , (S3) the linear response region of the amplified shift Δ with θ_K , and (S4) a comparative experimental case to measure the complex MOKE using the standard polarimetry scheme.

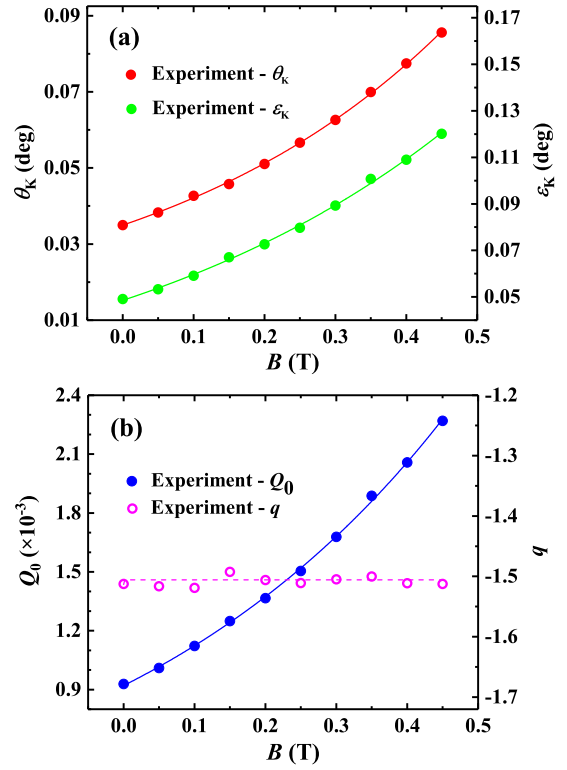


FIG. 5. The dependence of the complex MOKE parameters on the intensity of the magnetic field. (a) θ_K and ε_K , (b) Q_0 and q . The scatterers are the calculated results according to Δ' and η , and the curves are the guides to the eye.

ACKNOWLEDGMENTS

This work is supported by National Natural Science Foundation of China (61871451), Sichuan Science and Technology Program (2022YFG0166), and Joint Fund of Bijie City and Guizhou University of Engineering Science (Bijie Science and Technology Union Contract [2023] No.16).

AUTHOR DECLARATIONS

Conflict of interest

The authors have no conflicts to disclose.

Data Availability

The data that support the findings of this study are available from the corresponding author upon reasonable request.

¹X. Qiu, X. Zhou, D. Hu, J. Du, F. Gao, Z. Zhang, and H. Luo, "Determination of magneto-optical constant of Fe films with weak measurements," *Appl. Phys. Lett.* **105**, 131111 (2014).

²C. You and S. Shin, "Generalized analytic formulae for magneto-optical Kerr effects," *Journal of Applied Physics* **84** (1998), 10.1063/1.368058.

- ³Z. J. Yang and M. R. Scheinfein, “Combined three-axis surface magneto-optical Kerr effects in the study of surface and ultrathin-film magnetism,” *Journal of Applied Physics* **74**, 6810–6823 (1993).
- ⁴J. Zak, E. R. Moog, C. Liu, and S. D. Bader, “Magneto-optics of multilayers with arbitrary magnetization directions,” *Phys. Rev. B* **43**, 6423–6429 (1991).
- ⁵H. J. Williams, F. G. Foster, and E. A. Wood, “Observation of magnetic domains by the Kerr effect,” *Phys. Rev.* **82**, 119–120 (1951).
- ⁶C. A. Fowler and E. M. Fryer, “Magnetic domains on silicon iron by the longitudinal Kerr effect,” *Phys. Rev.* **86**, 426–426 (1952).
- ⁷A. Berger and M. R. Puffall, “Generalized magneto-optical ellipsometry,” *Applied Physics Letters* **71**, 965–967 (1997).
- ⁸K. Mok, N. Du, and H. Schmidt, “Vector-magneto-optical generalized ellipsometry,” *The Review of scientific instruments* **82**, 033112 (2011).
- ⁹N. Imamura, S. Tanaka, F. Tanaka, and Y. Nagao, “Magneto-optical recording on amorphous films,” *IEEE Transactions on Magnetics* **21**, 1607–1612 (1985).
- ¹⁰Y. He, L. Luo, L. Xie, J. Shao, Y. Liu, J. You, Y. Ye, and Z. Zhang, “Detection of magneto-optical Kerr signals via weak measurement with frequency pointer,” *Opt. Lett.* **46**, 4140–4143 (2021).
- ¹¹T. Li, Q. Wang, A. Taallah, S. Zhang, T. Yu, and Z. Zhang, “Measurement of the magnetic properties of thin films based on the spin Hall effect of light,” *Optics Express* **28**, 29086–29097 (2020).
- ¹²Q. Wang, T. Li, L. Luo, Y. He, X. Liu, Z. Li, Z. Zhang, and J. Du, “Measurement of hysteresis loop based on weak measurement,” *Opt. Lett.* **45**, 1075–1078 (2020).
- ¹³L. Luo, T. Li, Y. Jiang, L. Fang, B. Liu, and Z. Zhang, “Estimation of Kerr angle based on weak measurement with two pointers,” *Opt. Express* **31**, 14432–14441 (2023).
- ¹⁴T. Li, L. Luo, X. Li, M. T. Dove, S. Zhang, J. He, and Z. Zhang, “Observation of the mixed magneto-optical Kerr effects using weak measurement,” *Opt. Express* **31**, 24469–24480 (2023).
- ¹⁵Y. Aharonov, D. Z. Albert, and L. Vaidman, “How the result of a measurement of a component of the spin of a spin-1/2 particle can turn out to be 100,” *Phys. Rev. Lett.* **60**, 1351–1354 (1988).
- ¹⁶O. Hosten and P. Kwiat, “Observation of the spin Hall effect of light via weak measurements,” *Science* **319**, 787–790 (2008).
- ¹⁷X. Zhou, Z. Xiao, H. Luo, and S. Wen, “Experimental observation of the spin Hall effect of light on a nanometal film via weak measurements,” *Phys. Rev. A* **85**, 043809 (2012).
- ¹⁸X. Ling, Z. Zhang, Z. Dai, Z. Wang, H. Luo, and L. Zhou, “Photonic spin-Hall effect at generic interfaces,” *Laser & Photonics Reviews* , 2200783 (2023).
- ¹⁹H. Chen, G. Liu, S. Zhang, Y. Zhong, J. Yu, Z. Chen, and W. Zhu, “Spin Hall effect of nonlinear photons,” *Laser & Photonics Reviews* , 2200681 (2023).
- ²⁰D. J. Starling, P. B. Dixon, A. N. Jordan, and J. C. Howell, “Precision frequency measurements with interferometric weak values,” *Phys. Rev. A* **82**, 063822 (2010).
- ²¹Y. Liu, Y. Zhang, Z. Xu, L. Zhou, Y. Zou, B. Zhang, and Z. Hu, “Ultra-low noise phase measurement of fiber optic sensors via weak value amplification,” *Optics Express* **30** (2022), 10.1364/OE.455588.
- ²²X.-Y. Xu, Y. Kedem, K. Sun, L. Vaidman, C.-F. Li, and G.-C. Guo, “Phase estimation with weak measurement using a white light source,” *Phys. Rev. Lett.* **111**, 033604 (2013).
- ²³R. Wang, S. He, and H. Luo, “Photonic spin-Hall differential microscopy,” *Phys. Rev. Appl.* **18**, 044016 (2022).
- ²⁴D. Li, T. Guan, F. Liu, A. Yang, Y. He, Q. He, Z. Shen, and M. Xin, “Optical rotation based chirality detection of enantiomers via weak measurement in frequency domain,” *Appl. Phys. Lett.* **112**, 213701 (2018).
- ²⁵J. Xiao, T. Tang, X. Liang, K. Liu, Y. Tang, J. Li, and C. Li, “Chirality and concentration detection of biomolecules based on spin Hall effect of light,” *Physics Letters A* **416**, 127692 (2021).
- ²⁶Y. Wang, S. Yang, Q. Zhang, Y. Chen, X. Hu, H. Zhang, and Z. Zhang, “Complete chiroptical signal detection using weak measurement with intensity-contrast-ratio pointers,” *APL Photonics* **8**, 126102 (2023).
- ²⁷R. Wang, J. Zhou, K. Zeng, S. Chen, X. Ling, W. Shu, H. Luo, and S. Wen, “Ultrasensitive and real-time detection of chemical reaction rate based on the photonic spin Hall effect,” *APL Photonics* **5**, 016105 (2020).
- ²⁸R. Zhao, X. Wang, P. Wang, X. Wu, X. Fang, Y. Zhang, and S. Li, “Experimentally monitoring of the rapid biomolecular hydrolysis reaction with optical weak measurement,” *Laser Physics* **32**, 125201 (2022).
- ²⁹O. S. Magaña-Loaiza, M. Mirhosseini, B. Rodenburg, and R. W. Boyd, “Amplification of angular rotations using weak measurements,” *Phys. Rev. Lett.* **112**, 200401 (2014).
- ³⁰S. Chen, X. Zhou, X. Ling, W. Shu, H. Luo, and S. Wen, “Measurement of the optical constants of monolayer MoS₂ via the photonic spin Hall effect,” *Applied Physics Letters* **118**, 111104 (2021).
- ³¹X. Zhou, L. Sheng, and X. Ling, “Photonic spin Hall effect enabled refractive index sensor using weak measurements,” *Scientific Reports* **8**, 1221 (2018).
- ³²S. Chen, X. Ling, W. Shu, H. Luo, and S. Wen, “Precision measurement of the optical conductivity of atomically thin crystals via the photonic spin hall effect,” *Phys. Rev. Applied* **13**, 014057 (2020).
- ³³T. Tang, Y. Tang, L. Bi, T. Kang, X. Liang, J. Qin, J. Li, L. Luo, and C. Li, “Highly sensitive real-time detection of phase change process based on photonic spin Hall effect,” *Applied Physics Letters* **120**, 191105 (2022).
- ³⁴Q. Qiu, Z. and S. D. Bader, “Surface magneto-optic Kerr effect,” *Rev. Sci. Instrum.* **71**, 1243–1255 (2000).
- ³⁵L. Luo, L. Xie, J. Qiu, X. Zhou, X. Liu, Z. Li, Y. He, Z. Zhang, and H. Sun, “Simultaneously precise estimations of phase and amplitude variations based on weak-value amplification,” *Applied Physics Letters* **114**, 111104 (2019).
- ³⁶J.-H. Huang, J. S. Lundeen, K. M. Jordan, A. C. Dada, G.-J. Wang, and X.-Y. Hu, “Weak-value-amplification enhancement of the magneto-optical Kerr effect in nanoscale layered structures,” *Phys. Rev. A* **108**, 033724 (2023).
- ³⁷R. A. Hajar, F. L. Zhou, and M. Mansuripur, “Magneto-optical measurement of anisotropy energy constants on amorphous rare-earth transition-metal alloys,” *Journal of Applied Physics* **67**, 5328–5330 (1990).
- ³⁸D. Weller, Y. Wu, J. Stöhr, M. G. Samant, B. D. Hermsmeier, and C. Chappert, “Orbital magnetic moments of Co in multilayers with perpendicular magnetic anisotropy,” *Phys. Rev. B* **49**, 12888–12896 (1994).
- ³⁹Y. He, L. Xie, J. Qiu, L. Luo, X. Liu, Z. Li, Z. Zhang, and J. Du, “Manipulating photonic spin accumulation with a magnetic field,” *Journal of Applied Physics* **125**, 023101 (2019).
- ⁴⁰H. Luo, X. Zhou, W. Shu, S. Wen, and D. Fan, “Enhanced and switchable spin Hall effect of light near the Brewster angle on reflection,” *Phys. Rev. A* **84**, 043806 (2011).
- ⁴¹L. Luo, Y. He, J. Zhu, L. Fang, B. Liu, and Z. Zhang, “Precise measurement of polarization variation using weak measurement with double pointers,” *IEEE Photonics Journal* **15**, 1–6 (2023).
- ⁴²S. Chen, X. Ling, W. Shu, H. Luo, and S. Wen, “Precision measurement of the optical conductivity of atomically thin crystals via the photonic spin Hall effect,” *Phys. Rev. Applied* **13**, 014057 (2020).